Real-time phase contrast MRI versus conventional phase contrast MRI at different spatial resolutions and velocity encodings

Pan LIU (liupanronald@hotmail.com)
CHU Amiens-Picardie: Centre Hospitalier Universitaire Amiens-Picardie https://orcid.org/0000-0003-0559-6432
Sidy FALL
University of Picardy Jules Verne: Universite de Picardie Jules Verne
Maureen AHIATSI
University of Picardy Jules Verne: Universite de Picardie Jules Verne
Olivier BALEDENT
CHU Amiens-Picardie: Centre Hospitalier Universitaire Amiens-Picardie

Research Article

Keywords: phase-contrast, echo-planar imaging, cine MRI, pulsatile flow, imaging phantom

Posted Date: April 8th, 2022

DOI: https://doi.org/10.21203/rs.3.rs-1334567/v2

Real-time phase contrast MRI versus conventional phase contrast MRI at different spatial resolutions and velocity encodings

Pan Liu[1,2], Sidy Fall[3], Maureen Ahiatsi [1], Olivier Baledent[1,2,3]

[1] CHIMERE UR 7516, Jules Verne University of Picardy, Amiens, France.

[2] Medical Image Processing Department, Amiens Picardy University Hospital, Amiens, France

[3] MRI Department, Jules Verne University of Picardy, Amiens, France

Keywords: phase-contrast; echo-planar imaging; cine MRI; pulsatile flow; imaging phantom

1. Introduction

Conventional phase-contrast magnetic resonance imaging (Conv-PC) is a non-invasive technique that can be used to measure blood and cerebrospinal fluid (CSF) velocities. Conv-PC was used by Moran in 1982 to study flow velocities in humans [1]. Since then, Conv-PC has become a particularly important technique for *in vitro* studies and *in vivo* quantifications of blood and CSF flows [[2][3][4][5][6][7][8][9][10][11]].

Unfortunately, Conv-PC is limited by its relatively poor time resolution; it can only provide flow measurements for an averaged heartbeat cycle, which is reconstructed from all the acquired heartbeat cycles and uses gating. It is now known that breathing can affect CSF and cerebral blood flows [[12][13]]. Consequently, the flow velocities measured with Conv-PC may be breathing-dependent. Furthermore, Conv-PC is difficult to reveal the effects of breathing on the dynamics of blood or CSF flows.

To overcome this limitation, several research groups have developed a fast acquisition method based on echo-planar imaging (EPI) in which a complete k-space can be acquired using one or a small number of pulse excitations [[14][15]]. Eichenberger et al. in 1995 combined EPI with phase-contrast technique and thus introduced a novel sequence now commonly referred to as EPI-PC, using which they successfully quantified the blood flow of thoracic vessels at 20mm diameter level in real-time with a spatial resolution of 5×5 mm^2 [16]. With improved hardware performance, higher spatial resolution and smaller velocity encoding (VENC) can recently be used in EPI-PC to quantify cerebrovascular blood flow with smaller cross-sectional areas and cerebrospinal fluid oscillations with slower flow rates in real-time. With a high time resolution (a sampling frequency of ~10 Hz), a shorter acquisition time, and a simpler acquisition process (i.e. no need for synchronization), EPI-PC has clear advantages in the field of research but also opens new opportunities for clinical practice. An increasing number of researchers are using EPI-PC to quantify the effect of respiration on cerebral circulation [[17][18]].

However, EPI-PC is more sensitive to eddy currents and has a longer readout window, resulting in a lower velocity-to-noise ratio (VNR) of the phase image than for Conv-PC [[19][20][21]]. Increasing pixel size can increase VNR while improving imaging speed, but it is also more likely to produce partial volume effects [22]. Using a larger VENC can avoid the aliasing effects, but it will reduce the VNR and thus increase the segmentation difficulty. A better understanding of the effects of spatial resolution and VNR on EPI-PC allows us to further ensure quantification accuracy and improve imaging quality. However, to the best of our knowledge, there is a lack of specific literature on this field.

The objectives of this *in vitro* study were to quantitatively evaluate the accuracy of EPI-PC vs. Conv-PC and to assess the influence of pixel size and VENC on flow rate measurements.

2. Material and Methods

2.1. Flow phantom

The phantom consisted of a series of four rigid, straight tubes (Tygon tubing, Saint-Gobain Performance Plastics, Akron, OH) with inner diameters of 9.5 mm (tube #1), 6.4 mm (tube #2), 4.4 mm (tube #3) and 2 mm (tube #4). The

fluid flow was generated using a pulsatile flow pump. Six meters of tubing carried the fluid from the pump (located in the scanner control room) to the phantom's inlet. The phantom's outlet was connected to the tank that supplied water to the pump (Fig. 1 a).

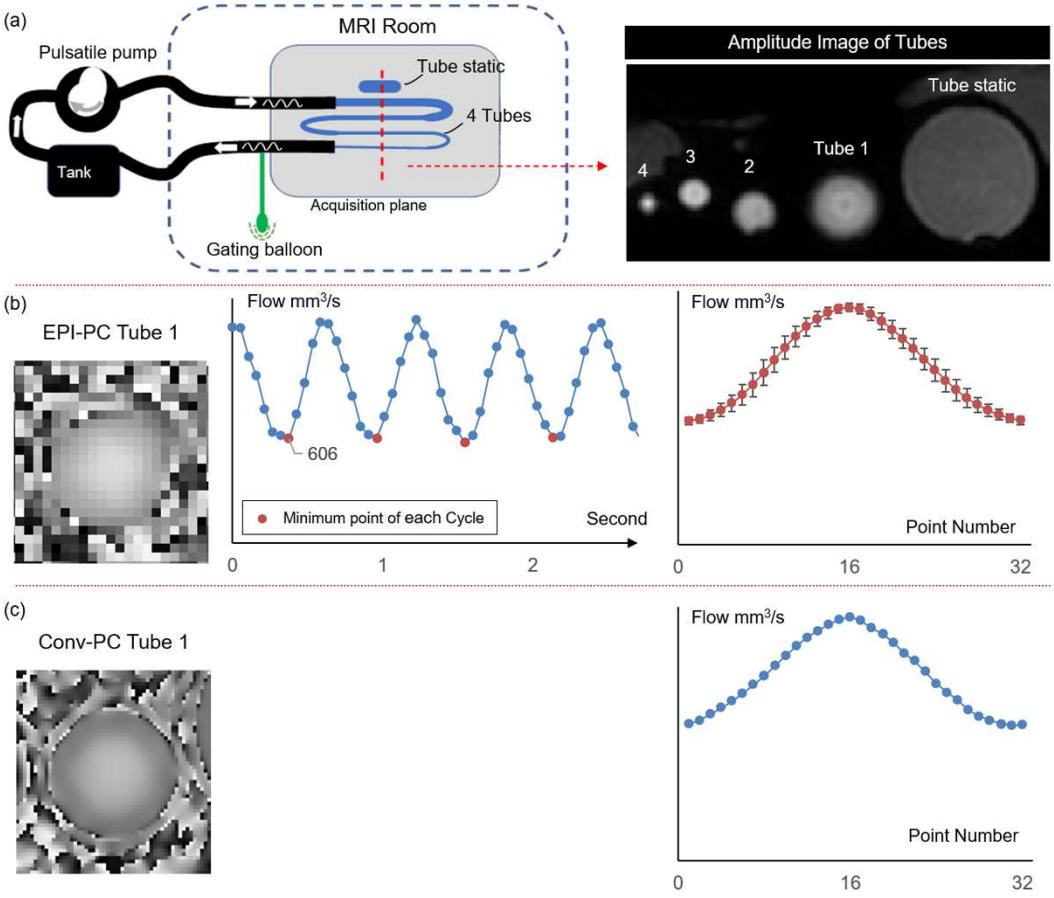

Fig. 1. The flow phantom and the flow curve for the two sequences. **a)** A realistic pulse-based model of the craniospinal system (left). An amplitude image for four tubes and a static tube in the acquisition plane (right), **b)** An EPI-PC phase image (left) and its calibrated flow curve (middle) with the minimum (trough) points (in red) in each cycle found automatically by the software, which are used to separate the cycles. All the EPI-PC pulse cycles were used to reconstruct an average pulse cycle (right), **c)** The Conv-PC phase image (left) and its calibrated flow curve.

To validate our system's flow rates, the pump was calibrated to deliver a clinically relevant flow rate (pulsatile flow with 99 bpm), and the volume collected from the phantom's output was recorded as a function of time. The true (calibrated) phantom flow rate (1150 mm^3/s) was obtained through repeated measurements and was used as the reference value for calculation of the EPI-PC's accuracy. The present work covered measurements obtained with the first tube (diameter: 9.5 mm) only.

The flow phantom was positioned in the center of a head coil. On the return tube, a gating-compliant balloon was used to capture the frequency of the oscillation and thus to synchronize the acquisition of the Conv-PC with the flow rate waveform. A water-filled tube (tube reference) was positioned beside the tubes, to define the static reference region.

2.2. Imaging procedure

All images were acquired on a 3T clinical scanner (Philips Achieva; maximum gradient: 80 mT/m; rate of gradient increase: 120 mT m^{-1} ms^{-1}). A 32-channel head coil was used to detect signals.

The EPI-PC sequence used in this experiment was a modified version of a standard, multi-shot, gradient-echo EPI sequence [23] with a Cartesian trajectory [[24][25]]. Typically, the velocity is encoded along the flow direction by positioning a bipolar gradient (with opposite polarity) behind the slice selection gradient. The spins of flowing tissue are at different locations relative to the bipolar gradient's positive and negative lobes. These spins are then confronted with the magnetic field gradients and accumulate a residual phase difference, whereas the stationary tissue does not experience a variation in the magnetic gradient. Phase data sets from before and after gradient reversal are subtracted to determine the "phase difference" of flowing spins, which is directly proportional to their underlying velocities. A description of the relationship between the measured phase and the velocities can be found in [26].

The imaging protocol parameters for both sequences are shown in Table 1, and the acquisition was repeated 10 times. EPI-factor is a parameter specific of EPI-PC that indicates the number of echoes acquired during a TR.

Each Conv-PC series contained 32 phase images after 23.6 seconds of acquisition, the interval between two images (Δt) during an average cycle was constant (Δt = 19 milliseconds). For EPI-PC series, the total number of acquired phase images was set to 150. The acquisition time is 9.3 seconds, and the Δt is 62 milliseconds.

Table 1. Default parameters for Conv-PC and EPI-PC.

	Conv-PC	EPI-PC
FOV (F×P)	100×60	100×60
VENC (cm/s)	5	5
Pixel size (mm^2)	1.2×1.2	1.2×1.2
Thickness (mm)	4	4
Flip angle (degree)	30	30
EPI factor	NA	9
SENSE	1.5	2.5
TR (ms)	11	15.2
TE (ms)	7.7	9.1
Acquisition time (s)	23.6	9.3
Number of images per cycle	32	9.7

FOV = field of view; VENC = velocity encoding; EPI = echo planar imaging; SENSE = sensitivity encoding; TE = echo time; TR = repetition time.

To assessed the effects of pixel size and VENC on flow rate measurements for both sequences, the pixel size was set from 0.8 mm to 3.2 mm in increments of 0.4 mm, and VENC was set from 5 cm/s to 25 cm/s in increments of 5 cm/s. The acquisition was repeated four times for both sequences under each parameter.

2.3. Postprocessing procedure

To extract the flow rate curves, the MRI data were processed with in-house software (Flow [[27][28]]). To minimize the effects of eddy current on the measurements, the velocity was calibrated by measuring the mean velocity in the tube reference (Fig. 2.a, green circle). Furthermore, to compare the two sequences, the EPI-PC flow rate signal was reconstructed over an average pulse cycle of 32 points with the same model as Conv-PC (Fig. 1.b). The post-processing procedure is as follows:

2.3.1. *Regions of interest*

By using the software's segmentation function, a region of interest (ROI) within the tube #1 (ROI-Tube) can be automatically segmented on the phase image. The value of the segmented area can then be recorded. Likewise, a ROI withing the static tube (ROI-Reference) was manually defined as the source of velocity noise (Fig. 2. a, green cycle). For each phase image, the mean (V_{Ref}) and standard deviation (SD) (σ_{Ref}) velocity within ROI-Reference were calculated. The V_{Ref} and σ_{Ref} values were used to define a reference signal and an uneven signal, respectively (Fig. 2. c & b).

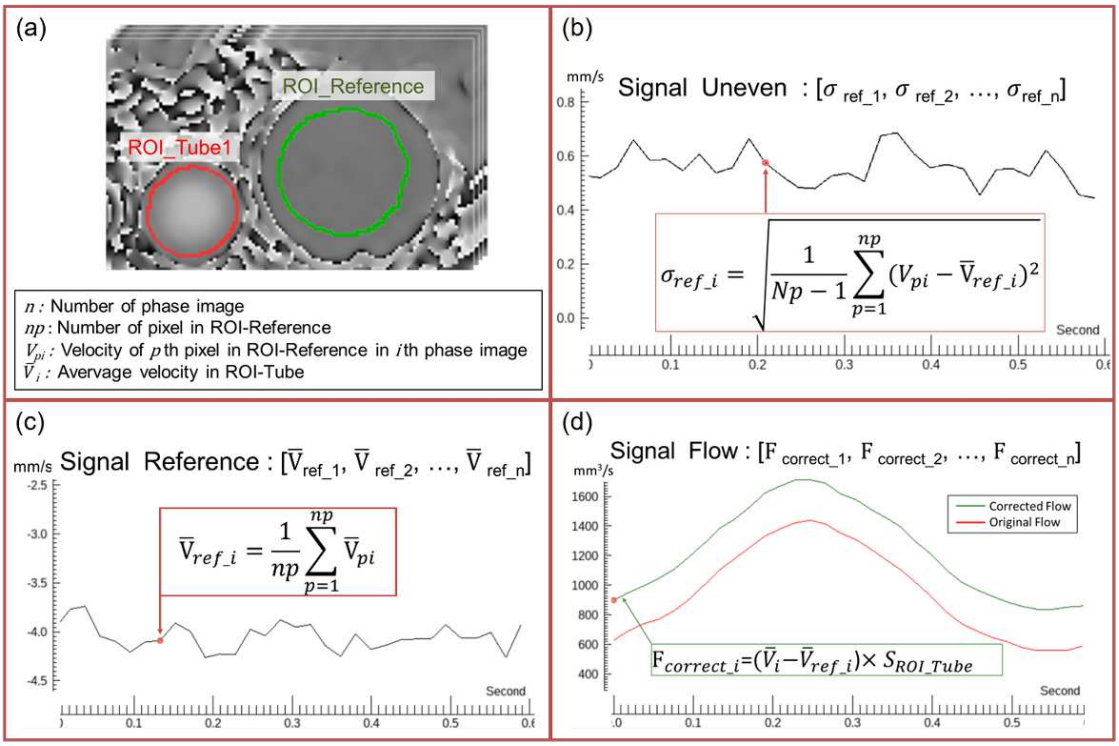

Fig. 2. An example of Conv-PC postprocessing. **a** A representative segmented image obtained with software, with ROI-Tube#1 on tube #1 (in red) and ROI-Reference on the static tube (in green), **b** The uneven signal obtained from the SD of the velocity within the ROI-Reference in each phase image, **c** The reference signal constituted by the mean velocity within the ROI-Reference in each phase image, **d** The original flow curve (in red) for a pulse cycle extracted from the ROI-Tube, and the corrected flow curve (in green) calculated from the original flow and reference signals.

2.3.2. *Calibration of the measured velocities*

The calibration compensated for the noise error in the measurement of velocity. In theory, the measured velocity does not represent the true velocity, and the velocity in the ROI-Reference is null. To calculate the corrected (true) velocity, the measured velocity was subtracted from the V_{Ref} (Fig. 2. d).

2.3.3. *Calculation of the VNR*

The mean uneven signal $\overline{\sigma_{Ref}}$ was used to calculate the VNR by dividing the mean velocity in the ROI-Tube by the mean uneven signal in ROI-Ref (equation 1).

$$VNR = \frac{\bar{V}}{\overline{\sigma_{Ref}}} \quad \ldots\ldots (1)$$

2.3.4. Reconstruction of the mean EPI-PC cycle

The steps in the segmentation and calibration of the EPI-PC data were the same as for the Conv-PC data (2.3.1 to 2.3.3). After the flow rate signal has been obtained from the EPI-PC data, the software's cropping tool can be used to extract all the single pulse cycles from the original signal (red points in Fig. 1. b). A spline interpolation algorithm was then used to increase the number of sampling points to 32 for each pulse cycle in the EPI-PC data. The sampling points at each position and each pulse cycles were then averaged to obtain the corresponding flow rate value for the reconstructed average pulse cycle. This average flow curve will be used for subsequent accuracy evaluations and analyses of the effects of pixel size and VENC.

2.3.5. The pulsatility index

Calculate the pulsatility index of flow curve of Conv-PC and the pulsatility index of average flow curve of EPI-PC using Equation 2.

$$Pulsatility\ index = \frac{Max\ flow - Min\ flow}{Mean\ flow} \quad \ldots\ldots (2)$$

2.4. Accuracy assessment of EPI-PC

The accuracy of EPI-PC was evaluated by comparing the quantified results of EPI-PC with the reference flow rate and reference area of calibrated phantom, and with the pulsatility index of the flow curve of Conv-PC.

2.5. The influence of pixel size and VENC

The measured average flow, segmentation area and VNR of the two sequences at different pixel sizes and velocity encodings were compared to analyze the effect of these two parameters on Conv-PC and EPI-PC. Based on literature procedures for measuring the accuracy of phase contrast sequences [[22][29]]. We considered that the acceptable confidence intervals (CIs) for the segmentation error and the flow rate error were ±10%.

2.6. Statistical analysis

The influence of pixel size and VENC on flow rate was evaluated using a regression analysis. Pearson's test was used to analyze the correlation between variables. Values are expressed as the mean ± standard deviation (SD). All statistical analyses were performed with R software (version 3.2.3, R Foundation for Statistical Computing, Vienna, Austria, www.r-project.org). The threshold for significance was set to $p<0.05$.

3. Results

After several manual measurements, it was verified that the average flow rate of the phantom was 1150 mm3/s. The Reynolds number of the tube #1 is 1260 and so was less than 2100, the flow was considered to be laminar.

3.1. Comparison of EPI-PC and Conv-PC sequences

The EPI-PC and Conv-PC sequences were applied to tube #1 with the default parameters.

After 10 measurements, the distributions of the average flow rate, segmentation area and pulsatility index of EPI-PC and Conv-PC are shown in Fig. 3. The mean flow rates for EPI-PC and Conv-PC were 1116±25 mm^3/s and 1239±26 mm^3/s respectively, and the associated coefficient of variation was 2.2% in both cases (Fig. 3. b). The segmentation areas of EPI-PC and Conv-PC were 70.1±1 mm^2 and 70±0.9 mm^2 respectively, and their coefficient of variations were 1.5% and 1.3% respectively (Fig. 3. c). The pulsatility indices for EPI-PC and Conv-PC were respectively 0.64±0.03 and 0.59±0.01 respectively, and their coefficient of variations were 2.5% and 4% respectively (Fig. 3. d).

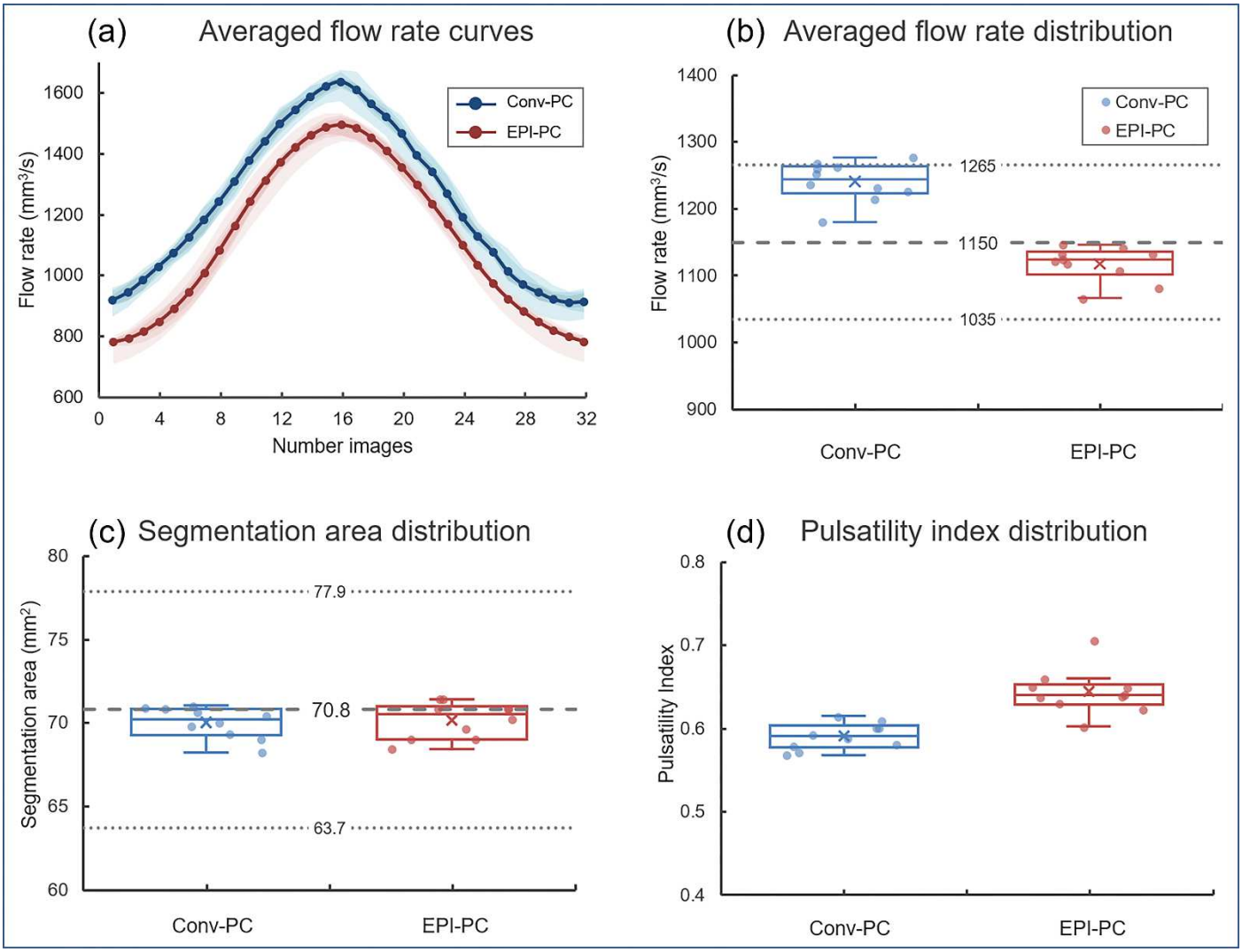

Fig. 3. a) The average flow curves for Conv-PC (in blue) and EPI-PC (in red). The distributions of the average flow rate b), segmentation area c) and pulsatility index d) of EPI-PC and Conv-PC. The lines segment (dashed) indicated the reference flow rate b) and the reference area c) of calibrated phantom, and the lines segment (dotted) indicated the CIs for flow rate and segmentation area.

3.2. The influence of pixel size

In Fig. 4, the segmentation area (blue points) and the flow rate (red points) are shown as a function of pixel size. Each variable was measured four times. The blue shading corresponds to the CI for the reference segmentation area (70.8 mm^2 ± 10%) and the red shading corresponds to the CI for the reference flow rate (1150 mm^3/s ± 10%). For both sequences, the segmentation area and flow rate were positively correlated with the pixel size. The coefficient (R^2) for the correlation between flow rate and pixel size was 0.79 ($P<0.01$) for EPI-PC and 0.9 ($P<0.01$) for Conv-PC. The

flow rates measurements obtained with EPI-PC were within the CI for pixel sizes of 1.2 mm to 2.8 mm. For Conv-PC, only pixel sizes of 1.2 mm to 2.4 mm provided flow rates within the CI.

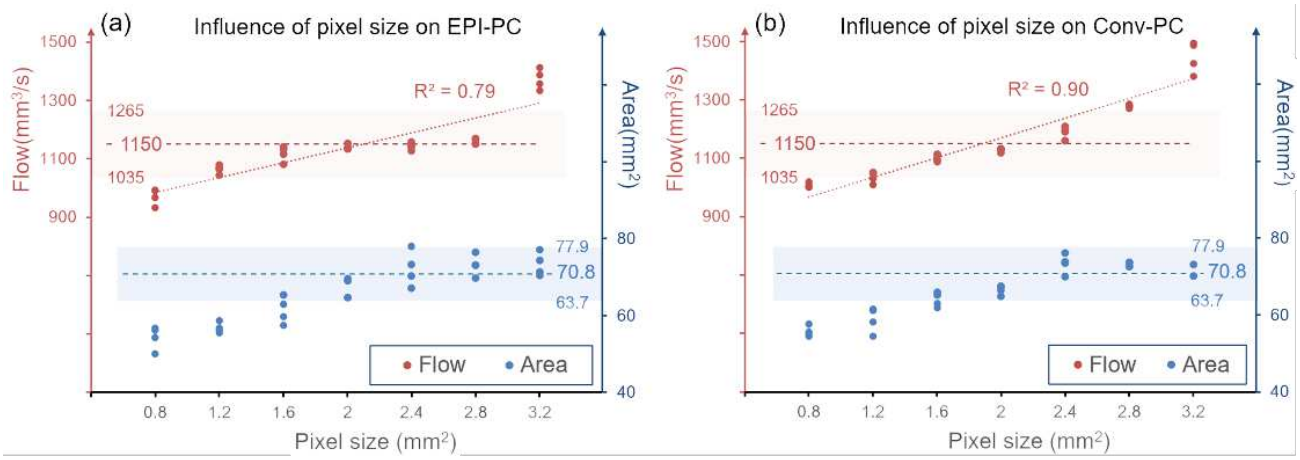

Fig. 4. Segmentation area (on the right y-axis, in blue) and flow rates (on the left y-axis, in red) for two sequences with different pixel sizes (on the X-axis). **a** EPI-PC, **b** Conv-PC

The distributions of the segmentation area (on the x axis) and flow rate (on the y axis) of the two sequences are shown in Fig. 5. The purple and green shadings correspond to the CI of the segmentation area and the flow rate, respectively.

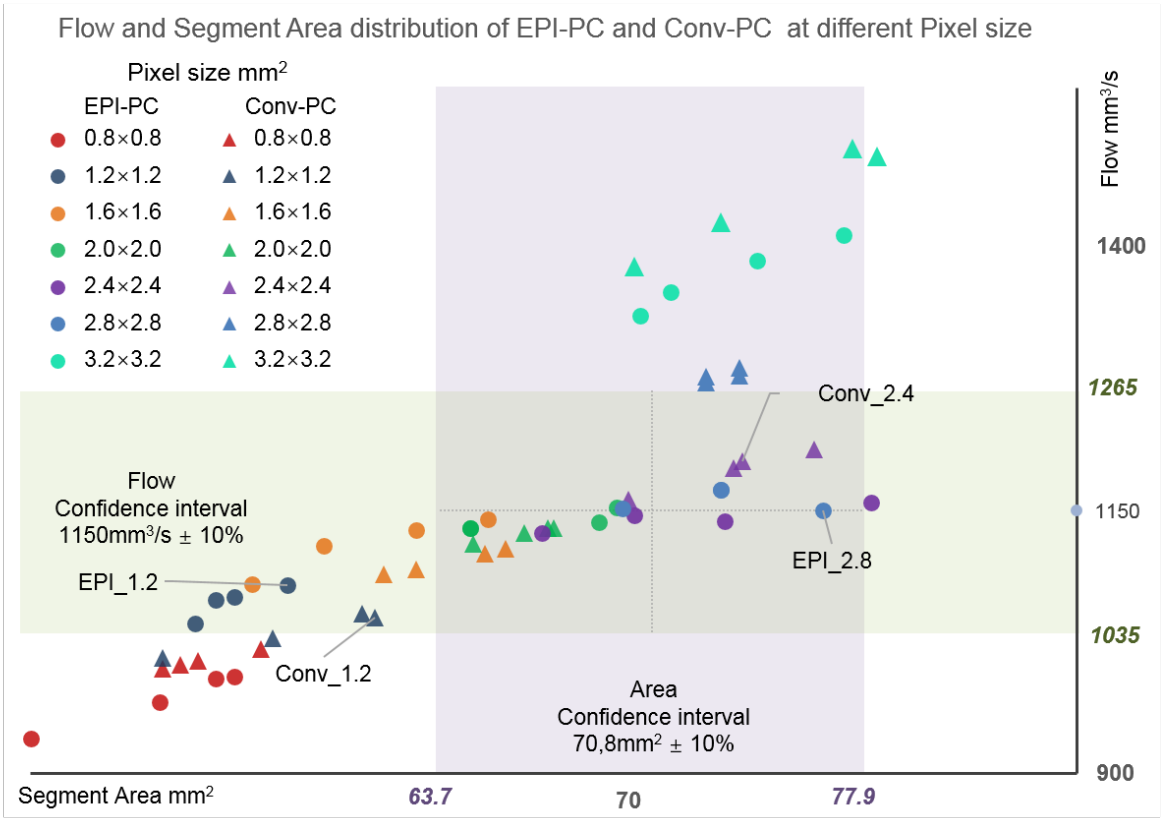

Fig. 5. Distribution of the segmentation area & flow rate for EPI-PC and Conv-PC, as a function of the pixel size (depicted by different color levels).

Fig. 6 shows the VNR of EPI-PC and Conv-PC with different pixel sizes. For a pixel size of 1.2 mm to 2.8 mm, the VNR increased for EPI-PC but did not change for Conv-PC. For each pixel size, the VNR was higher for Conv-PC than for EPI-PC.

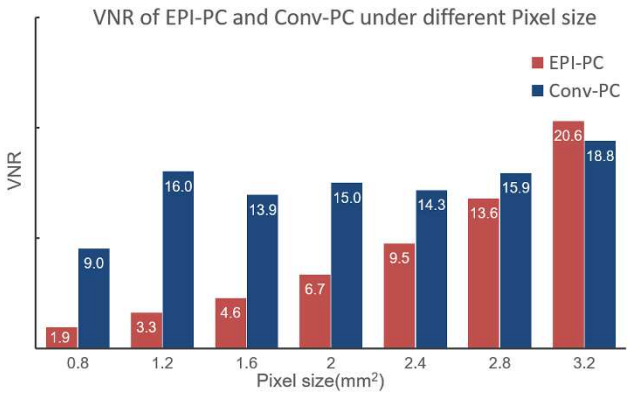

Fig. 6. The VNR for EPI-PC and Conv-PC sequences, as a function of the pixel size.

3.3. The influence of VENC

Fig. 7 shows the influence of VENC on EPI-PC and on Conv-PC. As the VENC increased, the accuracy decreased more rapidly for EPI-PC than for Conv-PC. With a VENC of 15 cm/s, the segmentation area for EPI-PC was outside the CI. Moreover, with a VENC of 20 cm/s, the flow rate for EPI-PC was also outside of the CI. For a VENC of 25 cm/s or more, the software was not able to segment the ROI. In contrast, with a VENC below 20 cm/s, the flow rates for Conv-PC were within the CI.

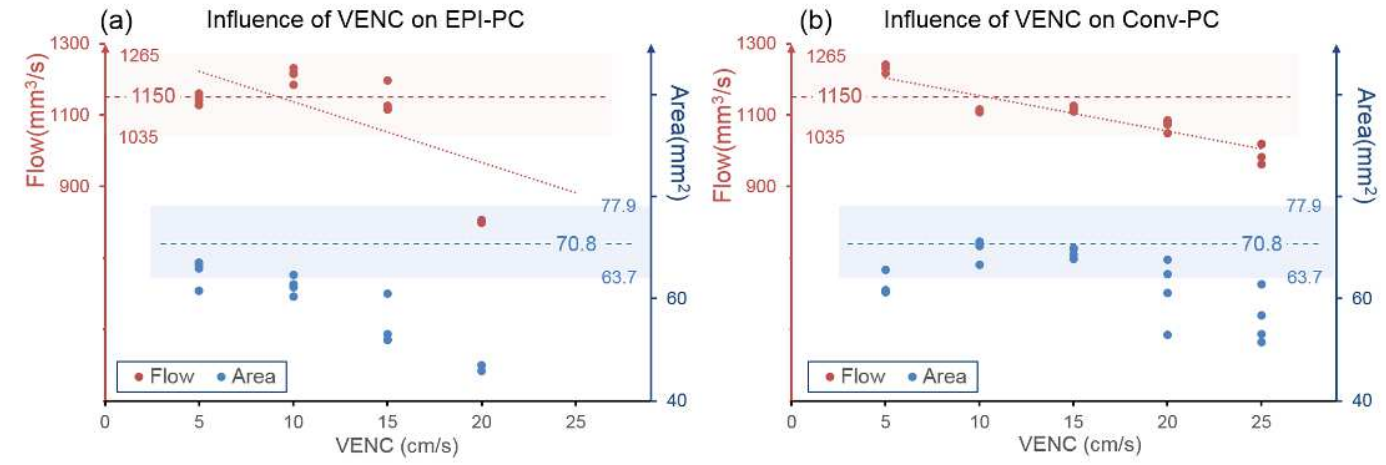

Fig. 7. Segmentation area (on the right y-axis, in blue) and flow rates (on the left y-axis, in red) for two sequences with five different VENC values (on the X-axis). **a** EPI-PC, **b** Conv-PC.

Fig. 8 gives the VNR for EPI-PC and Conv-PC with different VENC values. As the value of VENC increased, the VNR for EPI-PC fell from 3.6 to 0.8. For Conv-PC, the VNR fell from 27.2 to 8.1 as the VENC value increase from 5 cm/s to 15 cm/s. For VENC values of 15 cm/s to 25 cm/s, the VNR varied less (8.4 ± 0.76). Overall, the VNR with different VENC values was much greater for Conv-PC than for EPI-PC.

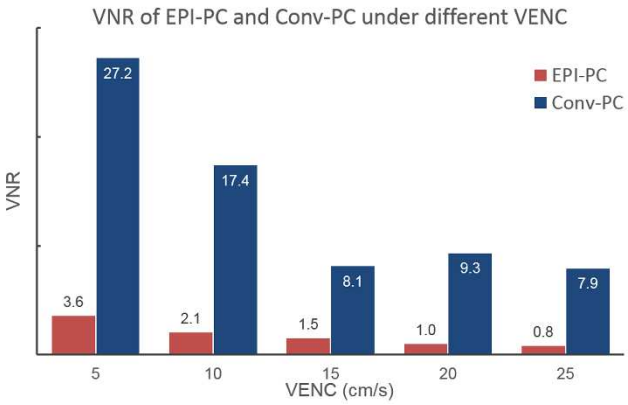

Fig. 8. The VNR for EPI-PC and Conv-PC sequences, as a function of the VENC.

4. Discussion

In the present study, we validated the accuracy of EPI-PC and evaluated the effects of spatial resolution and VENC on EPI-PC and Conv-PC.

The effects of magnetic field inhomogeneity must be taken account, since the reference tube was not positioned around the flow tube in the FOV [[30][31]]. Therefore, the estimated VNR in this study was a pseudo-VNR averaged across all images. This measurement method is likely to be more conveniently and might be sufficient for comparing the VNRs from several different sequences.

Single-shot EPI-PC has a higher sampling frequency but is more sensitive to geometric distortion and has a lower VNR [32]. The multi-shot EPI-PC is less sensitive to geometric distortions, given the shorter readout time [33]. This is why we used a multi-shot EPI-PC in this study.

4.1. Comparison of EPI-PC and Conv-PC

Using default parameters, the respective flow rate and segmentation area measurements for the two sequences were both within the CIs and did not exceed 8% [34] (flow rate error: -2.9% for EPI-PC vs. 7.8% for Conv-PC; segmentation area error: -1% for EPI-PC vs. -1.1% for Conv-PC). Difference in the pulsatility index between EPI-PC and Conv-PC was less than 10%.

The Conv-PC sequence was able to complete several phase encodings during each pulse cycle and to fill them into the different phase images' K-space; even though the acquisition time increased, it did not therefore affect the pseudo-sampling interval Δt. However, for the real-time imaging with EPI-PC, the acquisition time was directly related to Δt. The EPI-PC continue flow rate signal with default parameters, only 9 or 10 characteristic points were used to describe a pulse cycle. Therefore, EPI-PC is more suitable for flows with gentle fluctuations, such as venous blood and CSF. However, EPI-PC has limitations for reconstructing high-frequency fluctuations, such as certain arterial waveforms. Increasing the EPI-PC sampling frequency is likely to improve the accuracy of the corresponding reconstructed curve (Fig. S1).

4.2. The influence of pixel size

The EPI-PC sequence was less sensitive to pixel size than Conv-PC. Due to the characteristics of laminar flow, the velocity is lower at the boundary of the tube than in its center. When the resolution is high, the flow at the tube wall did not produce a large phase difference. Hence, this area can be considered to be non-flowing on the phase contrast image, and so the true segmented area is smaller than the theoretical area (Fig. 5).

Accurate segmentation area and flow rate measurements were possible with a range of pixel sizes: from 1.8 to 2.8 mm for EPI-PC and from 1.8 to 2.4 mm for Conv-PC. Within these ranges, the measured flow rate was slightly influenced by the segmentation area. As the pixel size continued to increase (above 2.8 mm for EPI-PC and above 2.4 mm for Conv-PC), the flow rate of the two sequences began to exceed the boundaries of the CI (Fig. 5). We hypothesize that a partial volume effect led to overestimation of the velocity [[22][35]]. As a result, the flow rate error was too large - even though the segmentation region was within the CI.

Therefore, in order to measure the flow rate accurately, the pixel size for Conv-PC should be less than 25% of the target ROI diameter; in other words, the ROI of Conv-PC should comprise at least 13 pixels. Our result is in line with those obtained by Greil et al. and Tang et al. [[22][29]], who confirmed that a minimum of 16 pixels within the Conv-PC ROI was required to keep the flow rate error within 10%. For the EPI-PC sequence, the pixel size should be less than 30% of the diameter of the target ROI diameter; in other words, the ROI of EPI-PC should have at least 9 pixels. On the other hand, while ensuring accuracy, larger pixel sizes can increase the VNR and improve imaging speed (Fig. S1), which is essential for EPI-PC.

4.3. The influence of VENC

The EPI-PC was more sensitive to VENC. Without aliasing, the VNR is inversely proportional to the VENC [[36][37]]. This sensitivity was also reflected in our experiments by the pseudo-VNR (Fig. 8 & Fig. S2). Compared to EPI-PC, Conv-PC can provide accurate flow rate with a larger VENC. Firstly, this was because the Conv-PC can use multiple cycles to fill a phase image, and so the influence of noise on the echo signal is smaller. For EPI-PC, multiple phase encodings are needed to complete the K-space during a TR, so the SNR of the echo signal is much smaller and the VNR of the phase image is relatively low. Secondly, in order to increase the sampling frequency in the EPI-PC sequence, the SENSE [38] value in this study as set to 2.5 which is 66% greater than that of Conv-PC (1.5), and a larger SENSE value decreases the VNR of phase image.

Since the VNR of Conc-PC was higher than that of EPI-PC, the increase in VENC had relatively little influence on the accuracy of Conv-PC flow rate measurements. Even when the VENC increased from 5 cm/s to 20 cm/s, the flow rate measured with Conv-PC was still within the CI. In contrast, the maximum value for VENC in the EPI-PC sequence was 10 cm/s; above this value, the segmentation was inaccurate.

The decrease in VNR mainly affects the segmentation of phase images; segmentation errors can arise when the pixel intensity in the phase image of the target vessel is close to that of the surrounding (non-flowing) tissue. This effect can be reduced if the magnitude image is used for segmentation.

On the other hand, a smaller VENC can increase the VNR, but at the same time slightly increasing the TR, leading to an increase in the Δt of EPI-PC (Fig. S3). Therefore, it is also feasible to improve the imaging speed by increasing the VENC in clinical applications while ensuring accurate quantification.

4.4. Limitations and perspectives

Firstly, the phantom waveform in our study was sinusoidal, whereas there are two higher-frequency harmonics (2-4 Hz) in the cerebral arterial waveform [39]. Hence, the ability of EPI-PC to accurately quantify the arterial waveform will now have to be demonstrated in *in vivo* studies. We encourage further investigation and validation of our findings.

Secondly, the phantom model did not take account of arrhythmic and respiratory effects, for which the EPI-PC sequence is advantageous because (in contrast to Conv-PC) it does not require synchronization with the cardiac cycle. Including these influences allows a more comprehensive comparison of the characteristics of the two sequences.

5. Conclusion

EPI-PC is considered as a valuable research tool to study the effect of respiration on cerebral circulation as it can provide beat-to-beat blood flow rate in real-time. Nonetheless, EPI-PC still has some limitations in quantifying cerebrovascular blood flow and cerebrospinal fluid oscillations. For example, its low VNR makes it more sensitive to VENC, and in order to obtain higher imaging speeds, EPI-PC tends to use larger pixel sizes making it easier to produce partial volume effects.

Our study shows that the calculated error between the reconstructed EPI-PC flow curve and the Conv-PC flow curve was small. Compared with Conv-PC, EPI-PC can be adapted to a lower spatial resolution but is more sensitive to VENC.

In this study, setting the pixel size of the EPI-PC to 30% of the diameter of the water tube gives the best VNR and temporal resolution without causing partial volume effects; and to obtain a higher VNR, VENC should be set small (aliasing needs to be avoided). These results provided reference values for the clinical application of EPI-PC.

List of abbreviations

Conv-PC: conventional cine phase-contrast MRI

CI: confidence interval

CSF: cerebrospinal fluid

EPI: echo-planar imaging

EPI-PC: phase-contrast echo-planar MRI

FOV: field of view

ROI: region of interest

ROI-Reference: ROI withing the static tube

V_{Ref}: mean velocity within ROI-Reference

σ_{Ref} : standard deviation velocity within ROI-Reference

VENC: velocity encoding

VNR: velocity-noise ratio

SD: standard deviation

SENSE: sensitivity encoding

SNR: signal-to-noise ratio

Δt: time interval between two images

References

[1] Moran PR. A Flow Velocity Zeugmatographic Interlace for NMR Imaging in Humans. Magn Reson Imaging. 1982;1(4):197-203.

[2] Bryant DJ, Payne JA, Firmin DN, Longmore DB. Measurement of Flow with NMR Imaging Using a Gradient Pulse and Phase Difference Technique. J Comput Assist Tomo. 1984;8(4):588-593.

[3] Feinberg DA, Mark AS. Human Brain Motion and Cerebrospinal Fluid Circulation Demonstrated with MR Velocity Imaging. Radiology. 1987;63(3):793-799

[4] Spraggins TA. Wireless Retrospective Gating: Application to Cine Cardiac Imaging. Magn Reson Imaging. 1990;8(6):675-681.

[5] Nayler GL, Firmin DN, Longmore DB. Blood Flow Imaging by Cine Magnetic Resonance. J Comput Assist Tomo. 1986;10(5):715-722.

[6] Greitz D, Franck A, Nordell B. On the Pulsatile Nature of Intracranial and Spinal CSF-Circulation Demonstrated by MR Imaging. Acta Radiol. 1993;34(4):321-328

[7] Alperin NJ, Sang HL, Lots F, et al. MR-Intracranial Pressure (ICP): A Method to Measure Intracranial Elastance and Pressure Noninvasively by Means of MR Imaging: Baboon and Human Study. Radiology. 2000;217(3):877-885.

[8] Balédent O, Gondry-Jouet C, Stoquart-Elsankariet S, et al. Value of Phase Contrast Magnetic Resonance Imaging for Investigation of Cerebral Hydrodynamics. J Neuroradiology. 2006;33(5):292-303

[9] McCauley TR, Pena CS, Holland CK, et al. Validation of Volume Flow Measurements with Cine Phase-Contrast MR Imaging for Peripheral Arterial Waveforms. J Magn Reson Imaging. 1995;5:663-68.

[10] Hoppe M, Heverhagen, JT, Froelich JJ, et al. Correlation of Flow Velocity Measurements by Magnetic Resonance Phase Contrast Imaging and Intravascular Doppler Ultrasound. Invest Radiol. 1998;33(8):427–432.

[11] Wåhlin A, Ambarki K, Birgander R, et al. Measuring Pulsatile Flow in Cerebral Arteries Using 4D Phase-Contrast MR Imaging. Am J Neuroradiol. 2013;34(9):1740-45.

[12] Schroth G, Klose U. Cerebrospinal Fluid Flow. II. Physiology of Respiration-Related Pulsations. Neuroradiology. 1992;35(1):10-15.

[13] Skytioti M, Sovik S, Elstad M. Respiration-Related Cerebral Blood Flow Variability Increases during Control-Mode Non-Invasive Ventilation in Normovolemia and Hypovolemia. Eur J Appl Physiol. 2017;117(11):2237-2249.

[14] Mansfield P. Multi-Planar Image Formation Using NMR Spin Echoes. J. Phys. C: Solid State Phys. 1977;10(3):55–58.

[15] Edelman RR, Wielopolski P, Schmitt F. Echo-planar MR imaging. Radiology. 1994;192(3): 600-612.

[16] Eichenberger AC., Schwitter J, McKinnon GC, et al. (1995). Phase-contrast echo-planar MR imaging: Real-time quantification of plow and velocity patterns in the thoracic vessels induced by valsalva's maneuver. J MAGN RESON IMAGING, 5(6), 648-655.

[17] Chen L, Vu AT, Xu S, et al. Evaluation of Highly Accelerated Simultaneous Multi-Slice EPI for FMRI. NeuroImage. 2015;104:452-459.

[18] Yildiz S, Thyagaraj S, et al. Quantifying the Influence of Respiration and Cardiac Pulsations on Cerebrospinal Fluid Dynamics Using Real-Time Phase-Contrast MRI. J Magn Reson Imaging. 2017;46(2):431-439.

[19] Kim, Y. J., Kim, S. H., Kang, B. J., Park, C. S., Kim, H. S., Son, Y. H., & Song, B. J. Readout-segmented echo-planar imaging in diffusion-weighted mr imaging in breast cancer: comparison with single-shot echo-planar imaging in image quality. Korean J Radiol. 2014;15(4):403-410.

[20] Wu W, & Miller KL. Image formation in diffusion MRI: a review of recent technical developments. J Magn Reson Imaging. 2017;46(3):646-662.

[21] Stanescu T, Wachowicz K., & Jaffray DA. Characterization of tissue magnetic susceptibility-induced distortions for MRIgRT. Medical Physics. 2012;39(12):7185-7193.

[22] Tang C, Blatter DD, Parker D. Accuracy of Phase-Contrast Flow Measurements in the Presence of Partial-Volume Effects. J Magn Reson Imaging. 1993;3(2):377-385.

[23] Romero JM, Liberato AC, Montes D, et al. Accuracy of MRI T2*-weighted sequences (GRE-EPI) compared to CTA for detection of anterior circulation large vessel thrombus. Emergency radiology. 2020;1-7.

[24] DeLaPaz, R. L. Echo-planar imaging. Radiographics. 1994;14(5):1045-1058.

[25] Benjamin, A. J. V., Gómez, P. A., Golbabaee, M., et al. Multi-shot Echo Planar Imaging for accelerated Cartesian MR Fingerprinting: an alternative to conventional spiral MR Fingerprinting. Magnetic resonance imaging. 2019; 61:20-32.

[26] Pelc NJ, Herfkens RJ, Shimakawa A, Enzmann DR. Phase Contrast Cine Magnetic Resonance Imaging. Magn Reson Q. 1991;7(4): 229-54.

[27] Balédent O, Henry-Feugeas MC, Idy-Peretti I. Cerebrospinal Fluid Dynamics and Relation with Blood Flow: A Magnetic Resonance Study with Semiautomated Cerebrospinal Fluid Segmentation. Invest Radiol, 2001;36(7): 368-377.

[28] Fall S, Pan L, Balédent O. A Semi-Automatic Software for Processing Real-Time Phase-Contrast MRI Data. In: VipIMAGE 2019. 2019;34: p. 22-28.

[29] Greil G, Geva T, Maier SE, Powell AJ. Effect of Acquisition Parameters on the Accuracy of Velocity Encoded Cine Magnetic Resonance Imaging Blood Flow Measurements. J Magn Reson Imaging. 2002;15:47-54.

[30] Ha H, Park KJ, Dyverfeldt P, et al. In Vitro Experiments on ICOSA6 4D Flow MRI Measurement for the Quantification of Velocity and Turbulence Parameters. Magn Reson Imaging. 2020;72:49-60.

[31] Dyverfeldt P, Bissell M, Barker AJ, et al. 4D Flow Cardiovascular Magnetic Resonance Consensus Statement. J Cardiovasc Magn R. 2015;17(1):1-19.

[32] Farzaneh F, Riederer SJ, Pelc NJ. Analysis of T2 Limitations and Off-Resonance Effects on Spatial Resolution and Artifacts in Echo-Planar Imaging. Magn Reson Med. 1990;14(1):123-139.

[33] Holdsworth SJ, Skare S, Newbould RD, et al. Readout-Segmented EPI for Rapid High-Resolution Diffusion Imaging at 3T. Eur J Radiol. 2008;65(1):36-46.

[34] Garg P, Westenberg JJM, et al. Comparison of Fast Acquisition Strategies in Whole-Heart Four-Dimensional Flow Cardiac MR: Two-Centre, 1.5 Tesla, Phantom and in Vivo Validation Study. J Magn Reson Imaging. 2018;47(1):272-281.

[35] Bouillot P, Delattre BMA, Brina O, et al. 3D Phase Contrast MRI: Partial Volume Correction for Robust Blood Flow Quantification in Small Intracranial Vessels. Magn Reson Med. 2018;79:129-140.

[36] Lee AT, Pike GB, Pelc NJ. Three-point phase-contrast velocity measurements with increased velocity-to-noise ratio. Magn Reson Med. 1995;33:122–126.

[37] Ha H, Kim GB, Kweon J, et al. Multi-VENC Acquisition of Four-Dimensional Phase-Contrast MRI to Improve Precision of Velocity Field Measurement. Magn Reson Med. 2016;75(5):1909-1919.

[38] Pruessmann KP, Weiger M, Scheidegger MB, Boesiger P. SENSE: sensitivity encoding for fast MRI. Magn Reson Med. 1999;42:952–962.

[39] Maier IL, Hofer S, et al. Carotid artery flow as determined by real-time phase-contrast flow MRI and neurovascular ultrasound: A comparative study of healthy subjects. EUR J RADIOL. 2018;106:38-45.